ISSN (Print) 1226-1750
ISSN (Online) 2233-6656
Journal of Magnetics 31(3), 403-415 (2026) https://doi.org/10.4283/JMAG.2026.31.3.403

Analysis of Temperature Variation in the Tooth Gaps of Magnetic Fluid Seals

Jiahao Dong[1]*, Bao Jin[1], Zhenfei Shen[2], and Zhenkun Li[3]*

[1]*Hebei key of Laboratory of Intelligence Equipment Digitalize Design and Process Simulation, Tangshan University, Tangshan 063000, China*
[2]*China Institute for Radiation Protection, Taiyuan 030006, China*
[3]*School of Mechanical Electronic and Control Engineering, Beijing Jiaotong University, Beijing 100044, China*

(Received 9 July 2026, Received in final form 17 September 2026, Accepted 18 September 2026)

Magnetic fluid seals are widely used in high-speed precision equipment for their zero leakage and low wear. However, at high speed, heat generated by shearing the magnetic fluid in the sealing clearance accumulates, and the viscosity-temperature coupling effect degrades its pressure resistance and service life. Systematic coupled heat transfer analysis under cooling is lacking. This study focuses on trapezoidal pole-tooth magnetic fluid seals. An axisymmetric finite element model is built using COMSOL with MATLAB, with an iterative heat source correction algorithm, to simulate temperature fields from 500 to 8000 rpm with and without cooling. Heat transfer pathways, heat flux density, and temperature rise patterns are analyzed and verified by high-speed test bench experiments. At 8000 rpm without cooling, the maximum temperature rise at the seal surface is 127 °C; with 20 °C water cooling, the gap temperature drops by 92 °C. Heat flux density in the cooling groove channel reaches 8×10^3 W/m², the primary heat dissipation route. The relative error between simulation and experiment is about 6%, attributed to empirical heat transfer coefficients and simplified tooth width models. The iterative coupled model effectively characterizes the thermal-viscous coupling behavior, offering theoretical support for thermal-structural optimization of high-speed magnetic fluid seals.

Keywords : magnetic fluid, temperature, sealing, simulation

1. Introduction

Magnetic fluid seals, characterized by their distinctive advantages such as zero leakage, minimal wear, extended service life, and environmental friendliness, are extensively employed in diverse industrial sectors, encompassing aerospace [1], armarium [2], precision instruments [3], and high-end chemical processing [4]. They stand as a core sealing technology that is highly appropriate for high-speed and high-precision operating conditions. In the practical operation of a magnetic fluid seal, the gap area formed between the pole teeth and the rotating shaft serves as the core area for sealing. The magnetic fluid creates a stable sealing film in this area, which plays a vital role in isolating media and preventing leakage [5]. Under complex operating conditions, the shear friction heat generated by the operation of high-speed equipment, environmental temperature fluctuations, and electromagnetic thermal effects all contribute to substantial dynamic temperature changes within the sealing tooth gap. Owing to the confined space of the tooth gap and restricted heat dissipation conditions, heat accumulation is highly probable, leading to localized abnormal temperature fluctuations. These temperature variations directly modify the physical properties and mechanical behavior of the magnetic fluid [6]. Therefore, a systematic investigation of the temperature variation patterns in the magnetic fluid seal clearance and a clarification of the characteristics of temperature evolution can clearly reveal the critical influence of temperature on the overall performance, operational stability, and service life of magnetic fluid seals. This has significant research value for optimizing seal structures and enhancing sealing reliability under extreme operating conditions.

As early as the 1970s, Rosensweig [7] established the fundamental theoretical framework for magnetic fluids. However, his research was exclusively centered on the thermodynamic characteristics of magnetic fluids and

©The Korean Magnetics Society. All rights reserved.
*Corresponding author: Tel: +86-13463558908
E-mail: dongjiahao@tsc.edu.cn (J. Dong);
Tel: +86-15201463447
E-mail: zhkli@bjtu.edu.cn (Z. Li)

© 2026 Journal of Magnetics

provided a qualitative description of the macroscopic temperature-dependent magnetization and viscosity behaviors of magnetic fluids. Significantly, neither experimental investigations nor theoretical modeling was conducted to elaborate on the coupling interaction between temperature rise and sealing performance within magnetic fluid sealing structures. Subsequently, Berkovsky [8] conducted experiments on convective heat transfer in vertical magnetic fluid layers, exploring how the relative orientation between horizontal magnetic field gradients and temperature gradients governs the fluid convection behavior, and derived quantitative relationships between the heat transfer characteristics and the operational parameters.

Fertman [9] pioneered experimental investigations into the thermal behavior of magnetic fluid seals as early as 1980, deriving semi-empirical analytical expressions for viscous power dissipation in single-stage seals featuring various pole-tooth geometries. The study analyzed the influence of heat flux density in pole teeth on the temperature distribution of the seal fluid film and established a simplified correlation to determine the required heat flux needed to reduce the maximum temperature of the magnetic fluid to a specified limit.

Lutset [10] carried out experimental research on low - temperature high-speed magnetic fluid seals for cryogenic turbine generators operating at a rotational speed of 60 m/s and within a wide temperature range from -50 to 150 °C, aiming to meet the high-vacuum rotor sealing requirements. The study systematically examined the influences of magnetic circuit configuration, linear velocity, temperature, and shaft vibration on the maximum pressure-bearing performance of the seal. Although low-temperature conditions can expand the allowable operating speed of the seal, they notably increase the fluid viscosity, thus enhancing the viscous friction and heat generation in the clearance. Experimental results suggest that the optimal operating temperature range for stable seal performance is between -40 and 0 °C. When the temperature reaches the 90–140 °C range, the magnetic fluid is likely to boil and experience particle agglomeration, eventually resulting in seal failure. Constrained by the testing conditions at that time, this study only determined the applicable temperature range from a macroscopic viewpoint, without conducting a detailed analysis of the internal temperature distribution within the seal clearance.

Kurfess [11] developed a high - speed sealing test platform to conduct an experimental investigation into the effects of operating parameters, including temperature and rotational speed, on the durability of magnetic fluid seals. Throughout the tests, the temperatures of pole shoes and the maximum pressure resistance values were concurrently recorded to analyze the fundamental mechanisms through which temperature conditions influence seal failure modes. The study reveals that temperature variations modify the viscosity of the sealing medium, thus indirectly impacting the interfacial flow rate between the two phases within the seal clearance and the critical rotational speed for interface instability. Moreover, the paper explicitly indicates that existing theoretical models for interface instability fail to consider thermal coupling effects, leading to substantial limitations in quantitatively predicting the performance evolution caused by temperature changes.

With the rapid progress of numerical computation techniques, a multitude of researchers have carried out numerical analyses on the temperature evolution patterns within magnetic fluid seal gaps by means of multi-physics simulation tools. Cheng [12] developed a mathematical computational model that is capable of calculating the peak temperature of high - speed sealed magnetic fluid films. The model emphasizes the necessity of incorporating the rheological properties of the medium in high - temperature condition predictions. Moreover, this model offers a theoretical foundation for the thermal structural design and performance assessment of magnetic fluid seals. Nesterov [13] formulated a numerical model that couples the magnetic field, fluid flow, and temperature fields to analyze the viscous heat generation characteristics within high-speed rotating shaft magnetic fluid seals. Subsequently, the accuracy of the model was validated using experimental data. The results indicate that when the surface linear velocity of the shaft attains 25 m/s, the heat generated by viscous shear can lead to an overall temperature increase in the magnetic fluid exceeding 80 °C.

Temperature is a crucial factor that determines the pressure resistance performance limit of magnetic fluid seals. The majority of existing research centers on the simulation and optimization of seal magnetic circuit structures. In contrast, numerical analysis of the temperature field in seals is comparatively scarce, and multi-field coupled simulations involving external cooling structures are even more infrequent.

To investigate the temperature evolution characteristics of the magnetic fluid seal clearance under high-speed operating conditions, a coupled COMSOL with MATLAB finite element simulation model was developed. This model incorporated a viscosity-temperature iterative correction algorithm to calculate the steady-state temperatures in the seal. Numerical simulations of the temperature fields were performed under various conditions, such as with and without cooling structures, and at multiple

rotational speed levels. This enabled a comprehensive analysis of the temperature distribution within the seal clearance. Subsequently, dynamic performance experiments were conducted. The measured temperature data were compared with the simulated temperature data to verify the accuracy of the finite element model and confirm the reliability of the coupled iterative simulation method.

2. Magnetic Fluid Sealing

2.1. Sealing structure

The magnetic fluid sealing structure employed in this study is presented in Fig. 1. Under the influence of a closed magnetic circuit constituted by permanent magnets, pole shoes, pole teeth, and the rotating shaft, the magnetic fluid is stably confined within the sealing clearance to form several liquid sealing rings, which act as wear-free liquid oil seals. The multi-stage liquid rings formed by a series of pole teeth share the pressure difference on both sides stage by stage.

The sealed housing is constructed from UNS S31603 stainless steel, which possesses non - magnetic characteristics and efficiently mitigates magnetic leakage losses within the sealing system. The pole shoes and the shaft function as core magnetic components within the closed magnetic circuit, and their magnetic permeability directly dictates the maximum pressure resistance of the sealing structure. Soft magnetic materials are distinguished by narrow hysteresis loops, low residual magnetism, low coercive force, and high magnetic permeability. Moreover, the pole shoes necessitate machining to create cooling channels, whereas the shaft requires processing to form pole teeth. Taking into account these combined forming and machining requirements, both components are fabricated from soft magnetic alloys with outstanding overall processability. When comparing AISI 1045 and UNS S42000, the former exhibits marginally better magnetic properties, yet UNS S42000 provides superior machinability and corrosion resistance. Consequently, both the pole shoes and the rotating shaft in this device are uniformly chosen as UNS S42000. The magnetic source utilizes N35 neodymium iron boron permanent magnets, and the bearing that supports the rotating shaft is a Japanese NSK 6208DDU deep groove ball bearing.

Under high-speed operating conditions, magnetic fluid seals are susceptible to fluid leakage as a result of centrifugal force. When pole teeth are positioned on the pole shoes, centrifugal force leads to the accumulation of a substantial volume of magnetic fluid in the gaps between the teeth and at the tooth roots, thereby undermining the integrity of the sealing film. Conversely, when pole teeth are arranged on the rotating shaft, centrifugal force propels the magnetic fluid towards the tips of the teeth, causing less negative impact on the pressure - bearing performance of the seal [14]. Therefore, this study selects to machine pole teeth on the rotating shaft surface, setting the sealing clearance between the tip of the pole teeth and the inner bore of the pole shoe at 0.1 mm, with a trapezoidal tooth profile adopted. Compared to other tooth shapes, trapezoidal teeth effectively reduce

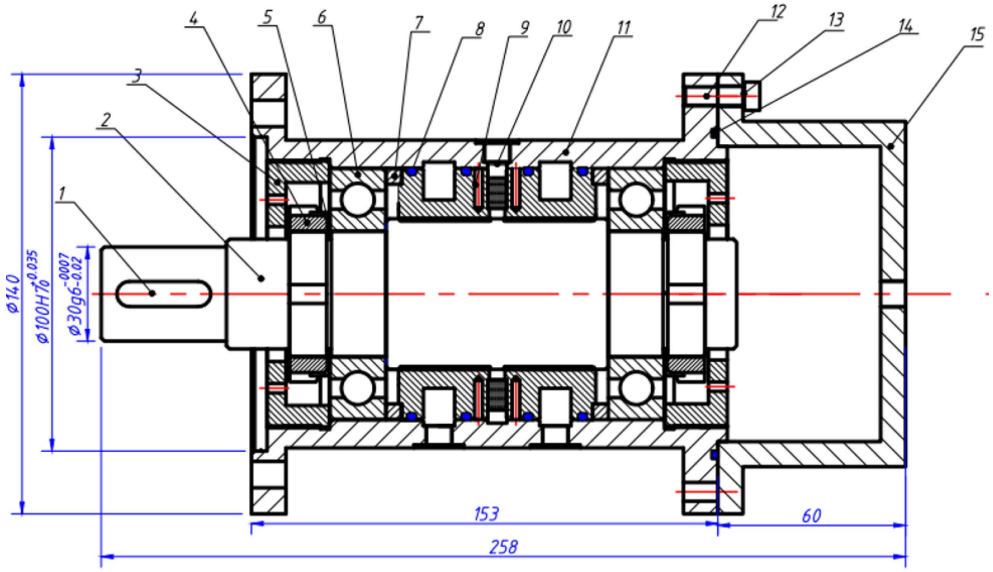


Fig. 1. (Color online) Magnetic fluid seal structure (Unit: mm)
1-Flat key; 2-Shaft; 3-End closure; 4-Circular nut; 5-Stop washer; 6- bearing; 7-Spacer sleeve; 8-O-ring; 9-Pole shoe; 10-Permanent magnet; 11-Housing; 12-Bolt; 13-Spring washer; 14-O-ring; 15-Sealing chamber.

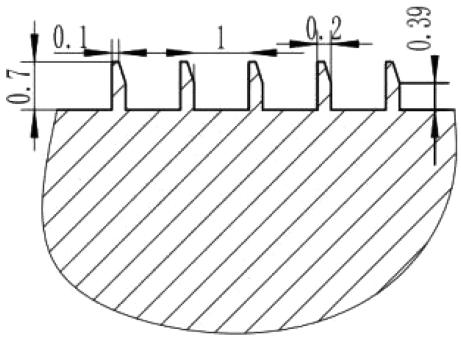


Fig. 2. The specific dimensional data of the pole teeth (Unit: mm).

local shear-generated heat, resulting in lower temperature rise within the sealing clearance under the same rotational speed, thereby slowing down the deterioration of magnetic fluid properties and extending the high-speed service life of the seal. To fully utilize the axial space of the shaft and enhance overall pressure resistance, a total of 40 trapezoidal pole teeth are arranged along the shaft, as shown in detail in Fig. 2.

2.2. Magnetic fluid

The magnetic fluid functions as the core sealing medium, and the saturation magnetization intensity and viscosity have a significant impact on the sealing performance. The magnetic fluid employed in this study was self-prepared in the laboratory and demonstrates superior saturation magnetization properties when compared to commercial magnetic fluids. The detailed preparation process and characterization analysis have been documented in previous literature [15].

An external magnetic field has the potential to induce the aggregation of nanoscale magnetic particles within a magnetic fluid, leading to the formation of chain-like or columnar structures that augment flow resistance. Temperature variations regulate molecular thermal motion and intermolecular forces, thereby resulting in the temperature-dependent viscosity behavior of the magnetic fluid at a macroscopic level.

The viscosity of magnetic fluids exhibits pronounced temperature dependence; consequently, thermal fluctuations can significantly influence viscous heat generation and the overall sealing efficacy of magnetic fluid seals. We conducted rheological tests on magnetic fluids using an Anton Paar rotational rheometer to systematically analyze the material's viscosity-temperature characteristics. The resulting viscosity versus temperature curve is shown in Fig. 3. A constant external magnetic field of 300 kA/m was maintained throughout the experiment, and a shear rate of 1000 s^{-1} was applied to replicate the high-shear

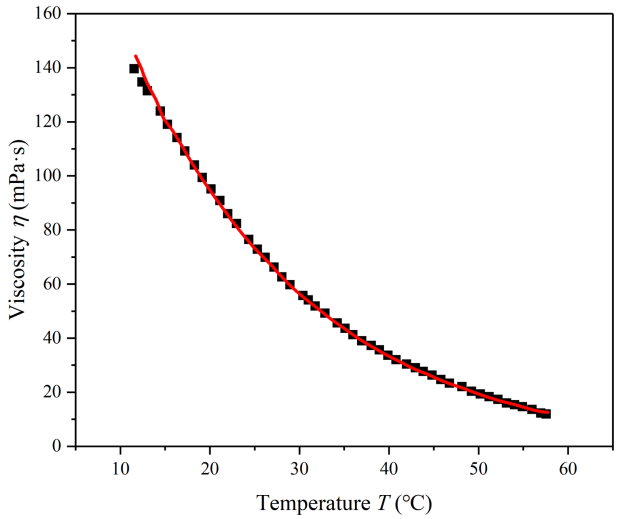


Fig. 3. (Color online) Viscosity-temperature relationship curve of magnetic fluid.

hydrodynamic conditions prevailing within operational sealing gaps. Temperature was incremented in precise 1 °C steps across the designated test range, and steady-state viscosity values were recorded only after thermal and rheological equilibrium was confirmed at each setpoint. This protocol ensured a high-resolution, continuous viscosity–temperature profile under the specified magneto-mechanical boundary conditions, yielding rigorously validated input parameters for coupled thermal and fluid-dynamic simulations.

To quantitatively characterize the variation of magnetic fluid viscosity with temperature, we selected the Navier-Stokes model to perform nonlinear fitting of the experimentally measured viscosity -temperature data [16].

$$\eta = \frac{S}{(a+T)^m} \tag{1}$$

According to the measurement curve, the fitting result of the simulation is:

$$\eta = \frac{1.511\times10^{13}}{(T+73.15)^{5.623}} \tag{2}$$

3. Thermodynamic Theoretical Analysis

3.1. Heat transfer mechanism of sealing devices

Heat transfer encompasses three fundamental mechanisms: conduction, convection, and radiation [17]. Inside the confined space of a closed device, heat exchange predominantly takes place via conduction and convection, whereas the contribution of thermal radiation is typically

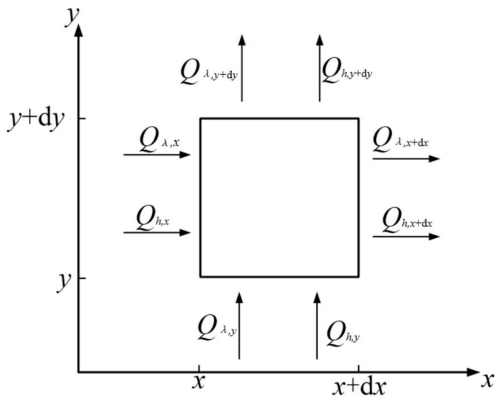


Fig. 4. Convective heat transfer models and thermal conduction models in microfluidics.

negligible.

By applying the micro - element energy conservation method to conduct a theoretical analysis of heat transfer processes, a two-dimensional model is established to couple conduction and convective heat transfer for simplified calculations. Consider a differential control volume *dxdy* within the region, as depicted in Fig. 4. Its energy conservation equation can be formulated as:

$$Q_{in} - Q_{out} + Q_v = dE \tag{3}$$

Where, Q_{in} is the energy that enters a differential element through its interface from all directions per unit time, Q_V is the power of the internal heat source within the microelement, Q_{out} is the energy per unit time departing from a differential element via the interface in all directions, *dE* is the rate of change of energy within a differential volume per unit time.

The energy entering and leaving the differential control volume through conduction can be expressed as:

$$Q_{\lambda,in} = Q_{\lambda,x} + Q_{\lambda,y} \tag{4}$$

$$Q_{\lambda,out} = Q_{\lambda,x+dx} + Q_{\lambda,y+dy} \tag{5}$$

Where, $Q_{\lambda,x}$ and $Q_{\lambda,y}$ denote the energy that enters the infinitesimal body in the *x* and *y* directions via heat conduction. $Q_{\lambda,x+dx}$ and $Q_{\lambda,x+dy}$ denote the energy that exits the infinitesimal body in the *x* and *y* directions via heat conduction.

In the heat conduction model, based on Fourier's law, it is stated that:

$$Q_{\lambda,x} = -\lambda F_x \frac{\partial t}{\partial x} \tag{6}$$

$$Q_{\lambda,y} = -\lambda F_y \frac{\partial t}{\partial y} \tag{7}$$

$$Q_{\lambda,x+dx} = -\lambda F_x \frac{\partial\left(t + \frac{\partial t}{\partial x}\right)}{\partial x} \tag{8}$$

$$Q_{\lambda,y+dy} = -\lambda F_y \frac{\partial\left(t + \frac{\partial t}{\partial y}\right)}{\partial y} \tag{9}$$

Where, λ is the thermal conductivity, *F* is the heat dissipation area of each surface of the microelement.

By summing up the heat flux income and expenditure at each boundary, the net heat input energy within the infinitesimal volume can be expressed as:

$$\Delta Q_\lambda = Q_{\lambda,in} - Q_{\lambda,out} = \lambda\left(\frac{\partial^2 t}{\partial x^2} + \frac{\partial^2 t}{\partial y^2}\right)dxdy \tag{10}$$

When the magnetic fluid sealing device is in operation, natural convection heat transfer takes place on the top surface of the housing, whereas the wall surface of the cooling slot experiences forced convection heat transfer as a result of the action of the cooling medium.

An analysis was conducted on the mechanism of forced convection in the cooling tank and natural convection in the shell. Theoretical derivation was performed by applying the principle of conservation of energy for infinitesimal elements. A two-dimensional flow simplification assumption was employed, and an infinitesimal element *dxdy* was selected in the (x,y) flow field. The mass of the fluid within the infinitesimal element was designated as *M*.

The mass that enters the infinitesimal body in the *x*-axis direction from the *x*-boundary within a unit of time is:

$$M_x = \rho u dy \tag{11}$$

The mass that leaves the infinitesimal body along the *x*-axis direction from the *x* + *dx* interface within a unit time is:

$$M_{x+dx} = M_x + \frac{\partial M_x}{\partial x}dx \tag{12}$$

By combining the two equations, the change in the static mass of the infinitesimal unit along the *x*-axis in a unit of time is:

$$\Delta M_x = M_x - M_{x+dx} = -\frac{\partial M_x}{\partial x}dx = -\frac{\partial(\rho u)}{\partial x}dxdy \tag{13}$$

Similarly, the change in the static mass of the infinitesimal unit along the *y*-axis in a unit of time is:

$$\Delta M_y = M_y - M_{y+dy} = -\frac{\partial M_y}{\partial y}dy = -\frac{\partial(\rho v)}{\partial y}dxdy \tag{14}$$

Therefore, the change in the static mass of the infinitesimal body per unit time is as follows:

$$\Delta M = \Delta M_x + \Delta M_y = -\frac{\partial(\rho u)}{\partial x}dxdy - \frac{\partial(\rho v)}{\partial y}dxdy = \frac{\partial \rho}{\partial \tau}dxdy \quad (15)$$

The net heat transferred to the infinitesimal element in the *x*-direction in a unit of time in the form of convection is:

$$\Delta Q_x = Q_x - Q_{x+dx} = -\frac{\partial Q_x}{\partial x}dx = -\rho c_p \frac{\partial(ut)}{\partial x}dxdy \quad (16)$$

The net heat transferred to the infinitesimal element in the *y*-direction in a unit of time in the form of convection is:

$$\Delta Q_y = Q_y - Q_{y+dy} = -\frac{\partial Q_y}{\partial y}dy = -\rho c_p \frac{\partial(vt)}{\partial y}dxdy \quad (17)$$

The net heat transferred to the infinitesimal element via convection within a unit time is as follows:

$$\Delta Q = \Delta Q_x + \Delta Q_y = -\rho c_p \left[u\frac{\partial t}{\partial x} + v\frac{\partial t}{\partial y} + t\frac{\partial u}{\partial x} + t\frac{\partial v}{\partial y} \right] dxdy \quad (18)$$

For two-dimensional steady flow with constant fluid density, the following relation holds:

$$\frac{\partial u}{\partial x} + \frac{\partial v}{\partial y} = 0 \quad (19)$$

Combining the aforementioned equations results in:

$$\Delta Q = -\rho c_p \left[u\frac{\partial t}{\partial x} + v\frac{\partial t}{\partial y} \right] dxdy \quad (20)$$

Let the volumetric heat generation inside the infinitesimal control volume be Q_V. The total heat variation of the control volume per unit time contributed by thermal conduction, convective heat transfer and internal heat generation is expressed as:

$$\Delta E = \left[\lambda\left(\frac{\partial^2 t}{\partial x^2} + \frac{\partial^2 t}{\partial y^2} \right) + Q_V \right] dxdy - \rho c_p \left[u\frac{\partial t}{\partial x} + v\frac{\partial t}{\partial y} \right] dxdy + Q_v \quad (21)$$

3.2. Magnetic fluid viscous heating

From an energy conservation standpoint, analysis of a magnetic fluid sealing system shows that although the rotating shaft gains kinetic energy, shear forces exerted by the magnetic fluid on the pole teeth give rise to viscous dissipation losses and interfacial friction losses. These losses are jointly converted into thermal energy, representing the dominant heat generation mechanism in magnetic fluid seals[12]. During operation, the tangential stress of the magnetic fluid within the sealing clearance is expressed as:

$$\tau_r = \eta\left(\frac{\partial V_\theta}{\partial r} + \frac{\partial V_r}{r\partial \theta} - \frac{V_\theta}{r} \right) \quad (22)$$

Leveraging the magnetic confinement effect inherent in the closed magnetic circuit, the magnetic fluid is stably retained within the sealing gap. In the idealized model, axial and radial flow of the magnetic fluid is neglected. Furthermore, under the assumption of negligible edge effects, the tangential velocity profile of the fluid film in the gap varies linearly with respect to the gap height, and the rotating shaft experiences only viscous shear forces from the magnetic fluid during operation. Based on these assumptions, the analytical expression for the viscous resistance torque L_τ is derived as follows [18]:

$$L_\tau = \sum_{i=1}^{n} \tau_{r,\theta} \cdot 2\pi r \cdot l_b \cdot r = \sum_{i=1}^{n} 4\pi l_b \eta \frac{\omega r_1^2 r_2^2}{r_2^2 - r_1^2} \quad (23)$$

Where, l_b is the tooth tip width of the pole tooth, η is the viscosity of the magnetic fluid, ω is the angular velocity of the rotating shaft, r_1 is the inner diameter of the sealing clearance, r_2 is the outer diameter of the sealing clearance.

Let the sealing gap thickness be denoted by $h = r_2 - r_1$. Since h is much smaller than the inner radius r_1, the foregoing equation admits a first-order approximation as follows:

$$\begin{aligned} L_\tau &= \sum_{i=1}^{n} 4\pi l_b \eta \frac{\omega r_1^2 r_2^2}{r_2^2 - r_1^2} = \sum_{i=1}^{n} 4\pi l_b \eta \frac{\omega r_1^2 (r_1 + h)^2}{h(r_1 + h + r_1)} \\ &\approx \sum_{i=1}^{n} 4\pi l_b \eta \frac{\omega r_1^4}{2hr_1} = \sum_{i=1}^{n} 2\pi l_b \eta \frac{\omega r_1^3}{h} \end{aligned} \quad (24)$$

Within the sealing clearance, the magnetic fluid undergoes circumferential flow, the resulting viscous shear torque dissipates mechanical energy, converting it into thermal energy. The corresponding expression for frictional power loss is given by:

$$P = L_\tau \cdot \omega = \sum_{i=1}^{n} 2\pi l_b \eta \frac{\omega^2 r_1^3}{h} \quad (25)$$

The heat flux density of each pole tooth is:

$$q = \frac{P}{A} = \frac{2\pi l_b \eta \dfrac{\omega^2 r_1^3}{h}}{2\pi r_1 l_b} = \eta \frac{\omega^2 r_1^2}{h} \quad (26)$$

Given the substantial temperature dependence of viscosity, the previously fitted viscosity - temperature equation of the magnetic fluid is incorporated into the above equation, leading to the simplified form:

$$q = \frac{1.511\times10^{13}}{(T+73.15)^{5.623}} \cdot \frac{\omega^2 r_1^2}{h} \tag{27}$$

4. Simulation Modeling

In this study, COMSOL and COMSOL with MATLAB are employed to calculate the temperature distribution of the magnetic fluid dynamic sealing device under operating conditions. The viscosity of magnetic fluids demonstrates notable temperature sensitivity, and the heat flux density produced by shear within the gap varies dynamically in accordance with the medium temperature. Once the system attains thermal equilibrium, both the viscosity and heat generation tend to reach a stable state, and the steady-state temperature becomes independent of the initial temperature. This study utilizes an iterative correction strategy, iteratively updating the input temperature T of the heat source and the solved temperature T' based on the viscosity-temperature relationship until all pole teeth satisfy the convergence criteria. The temperature finally obtained represents the steady-state temperature of the magnetic fluid considering the coupled viscous heating effects.

The native COMSOL environment does not support iterative correction of input temperature T and output temperature T'. Therefore, this paper adopts a combined simulation approach using COMSOL with MATLAB to achieve iterative solution of the steady-state temperature field in high-speed dynamic seals.

4.1. Model development

The sealing structure exhibits axisymmetric geometric characteristics. In order to reduce the computational scale, a two-dimensional axisymmetric model is employed for simulation analysis in this research. The model utilizes the z-axis as the rotational symmetry axis, and the geometric computational domain is presented in Fig. 5.

4.2. Material definition

Material density, thermal conductivity, and specific heat capacity at constant pressure are the crucial physical properties that govern the heat transfer process and the steady-state temperature distribution within a sealing system. The physical properties of all the components and magnetic fluids employed in this study are presented in Table 1. On the COMSOL with MATLAB coupled simulation platform, material databases for diverse materials

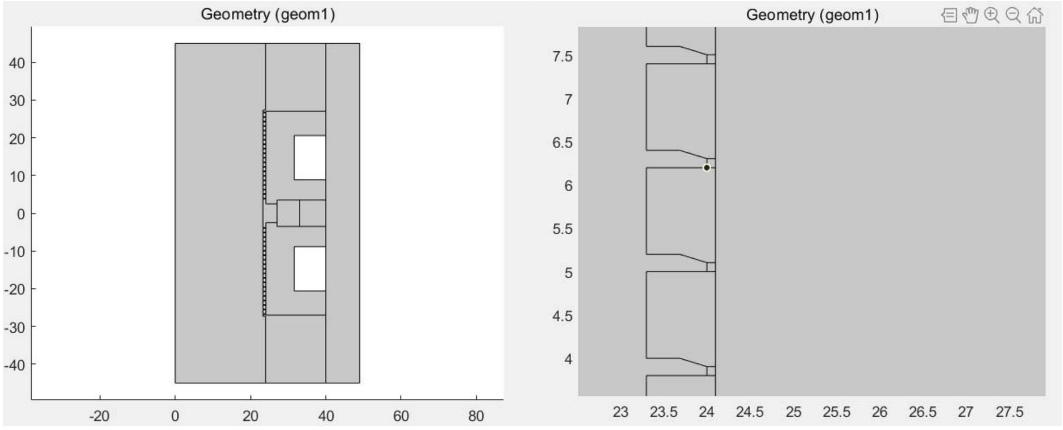


Fig. 5. Sealing Device Temperature Field Simulation Model.

Table 1. Material properties of sealing device.

Materials	Parts	Density (kg/m^3)	Thermal conductivity (W/(m·K))	Specific heat capacity (J/kg·K)
Permanent magnet	N35 Neodymium iron boron	7500	7	502
UNS S42000	Shaft; Pole shoe	7750	22.2	460
UNS S31603	Housing	7930	16.3	500
Sealing medium	Magnetic fluids	2050	0.2	1966
Air	Other region	1.205	0.0259	1005

were successively established, and the corresponding physical properties were allocated to the respective computational regions of the previously constructed geometric model via domain assignment operations.

4.3. Boundary conditions

The initial temperature boundary condition exerts a negligible influence on the solution of the steady-state temperature field. Therefore, the initial temperature across the entire domain is uniformly set to the room temperature of 20 °C.

Heat flux density is used to characterize the quantity of heat transferred per unit time and per unit area across an interface. In this model, the contact interface between the pole teeth and the magnetic fluid is regarded as a viscous heat generation source. Under high - speed shear conditions, the heat generated by viscous dissipation in the magnetic fluid is directly correlated with the medium temperature. The temperatures of the 40 contact surfaces between the pole teeth and the magnetic fluid, obtained through the solution, are substituted into eq. (27) in array form to compute the heat flux density at each interface, which is then incorporated into the multi-physics simulation model as parameters. The corresponding MATLAB code for applying heat flux density at a single interface is as follows:

```
for i=1:40
model.param.set(str1+num2str(i), num2str(q0(1,i)));
end
model.component('comp1').physics('ht').create('bhs1',
'BoundaryHeatSource', 1);
model.component('comp1').physics('ht').feature('bhs1').s
election.set([286]);
model.component('comp1').physics('ht').feature('bhs1').s
et('Qb', 'q1');
```

4.4. Mesh generation

The numerical solution of the heat transfer field utilizes triangular element meshing along with an adaptive mesh refinement strategy offered by the software. Given that both the pole teeth and the magnetic fluid region are associated with viscous heat generation and heat conduction, these regions undergo mesh refinement with the highest level of mesh density. The mesh discretization of the overall sealed model is presented in Fig. 6, with the total number of elements reaching 10992.

4.5. Data post processing

After the solution process, a two-dimensional characteristic cross-section is extracted along the radial direction, and all node temperature data on the cross-section are sampled at intervals of 0.05 mm. Subsequently, the exported dataset is post processed using MATLAB to obtain the temperature distribution patterns of the magnetic fluid at each pole tooth position.

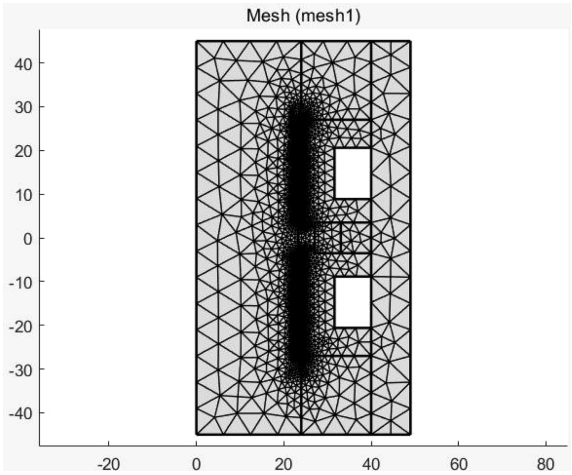


Fig. 6. Meshing results.

4.6. Adjust the temperature of the magnetic fluid

Adopt a correction coefficient of 0.5. Denote the initial input temperature of the heat source as T_1, and the interface temperature obtained from a single simulation as T_2. Utilize the weighted average temperature $0.5T_1 + 0.5T_2$ as the input temperature for the heat source in the subsequent iteration of the temperature field calculation. Substitute this value into eq. (27) to calculate the corresponding interface heat flux density, and then assign it to the model in array form for a new round of temperature field solution. The iterative process persists until the input and output temperatures at each pole tooth interface satisfy the preset convergence criterion, which is expressed as follows:

$$\sqrt{\left[\sum_{1}^{40}(T_2 - T_1)^2\right] / 40} / T_1 \le 0.15\% \tag{28}$$

The temperature field result T_2 derived from the solution denotes the steady-state temperature of the magnetic fluid when the system attains thermal equilibrium under operating condition ω, considering the viscosity-temperature coupling characteristics of the magnetic fluid.

5. Results

5.1. Simulation Results

By employing a coupled iterative algorithm that integrates COMSOL with MATLAB to solve the converged steady - state temperature of magnetic fluid at each pole tooth

position, the temperature results of each group are substituted into the theoretical formula for viscous heat generation heat flux density. Subsequently, the corresponding thermal load values for individual pole tooth interfaces are calculated. All the interface heat flux densities of the pole teeth are then imported in bulk into the COMSOL finite element model as array parameters, which facilitates the coupled global temperature field simulation and numerical analysis within the seal.

5.1.1. No cooling condition

The viscosity-temperature characteristics of ester-based magnetic fluids were fitted by means of the Navier-Stokes equation. The results indicated an overall decreasing trend in the medium's viscosity as the temperature increased. According to this equation, when the temperature surpasses 87 °C, the fluid's viscosity would fall below 6 mPa·s, which is inconsistent with engineering observations. Temperature is a reflection of the intensity of molecular thermal motion. An increase in temperature intensifies the Brownian motion of particles, thus reducing the relative rotational speed difference between the base liquid and magnetic nanoparticles. Nevertheless, once the temperature reaches a critical range, the enhancement of Brownian motion weakens considerably with further heating, resulting in a sharp decrease in the viscosity's sensitivity to temperature. Therefore, this study designates 70 °C as the critical viscosity threshold. Above this temperature, the viscosity of the magnetic fluid remains stable and does not change with the increasing temperature.

Set the rotational speed of the shaft to 8000 rpm, which corresponds to an angular velocity of 837.76 rad/s and a surface linear velocity of 20.1 m/s. Fig. 7 depicts the three-dimensional temperature distribution map of the sealing system under no cooling condition. When the ambient temperature is maintained at 20 °C, the maximum temperature rise in the sealing clearance under this condition can reach 127 °C. In the absence of external cooling structures, the system depends solely on natural convection between the housing and the surrounding air for heat dissipation, leading to low heat transfer efficiency and generally poor cooling performance.

As depicted in the temperature distribution results of the sealing clearance presented in Fig. 8, the high-temperature peak within the sealing system is concentrated at the interface where the magnetic fluid makes contact with the rotating shaft. This model takes into account only the viscous dissipation of the magnetic fluid as the sole internal heat source, with heat being transferred via conduction to the shaft, pole shoes, and the air within the seal cavity. The shaft, positioned at the center of the structure, can only dissipate heat outward through its two end-surfaces, leading to limited heat-dissipation pathways and extremely low cooling efficiency. The entire sealing unit is arranged horizontally in the axial direction, with natural convection taking place between the outer shell wall and the ambient air. During the process of radial heat conduction outward, a significant temperature gradient exists. The greater the temperature rise of the shell, the stronger the convective heat transfer at the outer wall, thus enhancing the total heat dissipation of the system.

The heat transfer paths of the sealed system are depicted in Fig. 9. Heat is predominantly dissipated externally via two channels: Path 1, from the magnetic fluid to the pole shoe, then to the housing, and finally to

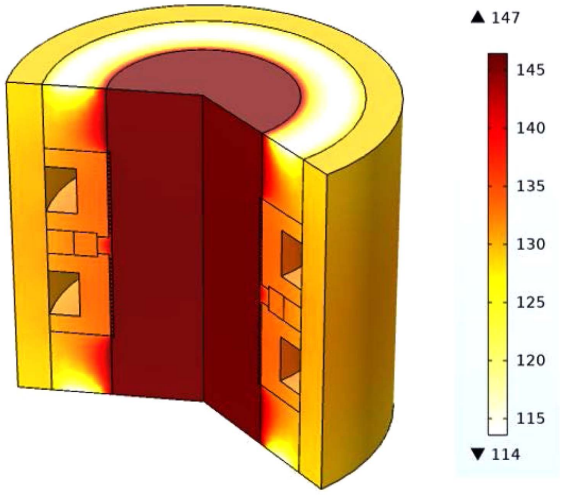


Fig. 7. (Color online) Three-dimensional temperature distribution contour map of the sealing device under no cooling condition.

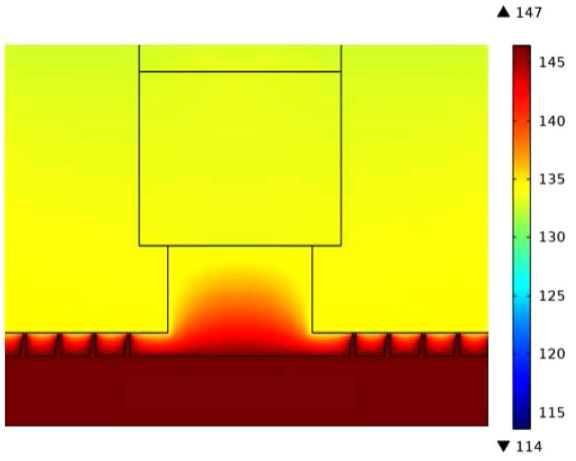


Fig. 8. (Color online) Two-dimensional temperature distribution contour map of the seal clearance under no cooling condition.

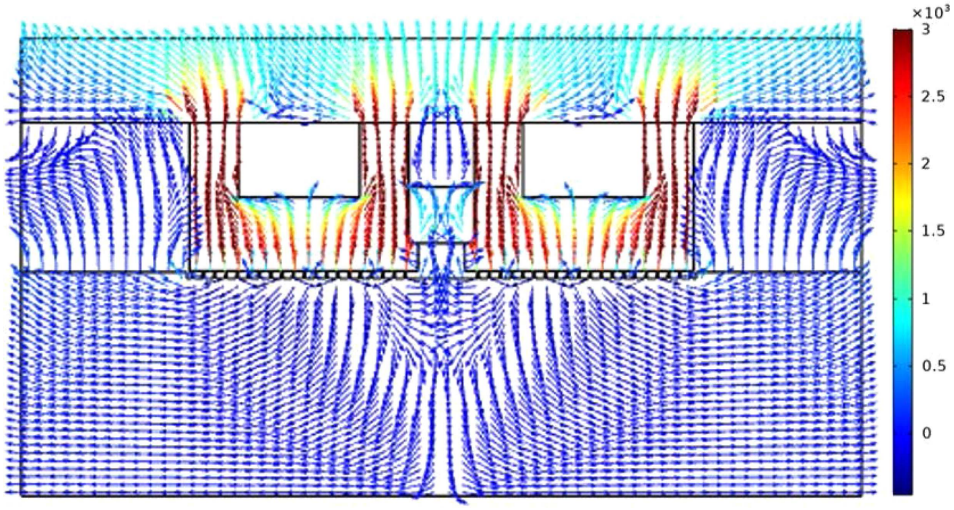


Fig. 9. (Color online) Vector map of heat flux density for the sealing device under no cooling condition.

the ambient air; and Path 2, from the magnetic fluid to the shaft and then to the ambient air. The medium filling both sides of the pole shoe is air, the thermal conductivity of which is significantly lower than that of UNS S42000. This leads to a considerably higher internal heat flux density within the pole shoe compared to the adjacent air regions. In Path 1, heat is mainly conducted through the pole shoe to the housing. Given that the conductive contact area between the pole shoe and the housing is smaller than the convective heat transfer area between the outer wall of the housing and the surrounding air, the heat flux density in the pole shoe region reaches its maximum value throughout the entire device, reaching 3×10^3 W/m^2, while the average heat flux on the outer surface of the housing is approximately 700 W/m^2.

5.1.2. Cooling condition

The temperature of the cooling water was kept constant at 20 °C, and the three-dimensional temperature distribution throughout the entire sealed system equipped with a cooling structure is presented in Fig. 10. Once the system achieved thermal equilibrium under this cooling condition, the maximum internal temperature of the seal was merely 54.9 °C, leading to an overall temperature increase of 34.9 °C relative to the 20 °C ambient environment. In comparison with the scenario without cooling, the forced heat transfer from the cooling channel effectively dissipated the heat generated by shear at the pole teeth, notably curbed the temperature rise of the magnetic fluid, and considerably enhanced the overall thermal environment of the seal. The temperature field of the sealing system demonstrates a typical axisymmetric distribution, with the temperature peak concentrated at the interface between

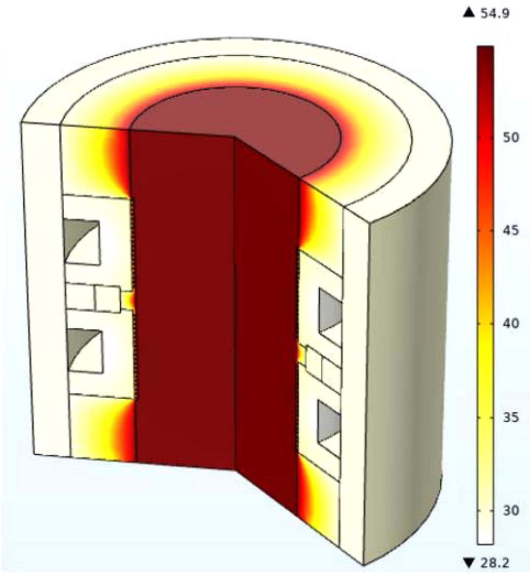


Fig. 10. (Color online) Three-dimensional temperature distribution contour map of the sealing device under cooling condition.

the magnetic fluid and the rotating shaft. This temperature distribution is attributed to the existence of a single heat source within the model, namely, the viscous dissipation heat generated by the shear action on the magnetic fluid under high-speed rotation conditions. At a rotational speed of 8000 rpm, the steady-state temperature in the seal clearance drops by 92 °C when cooled with 20 °C water as compared to the no cooling condition.

As depicted in the two-dimensional temperature distribution contour presented in Fig. 11, the temperature within the rotor shaft region maintains a relatively high level. Positioned at the center of the sealing structure, the

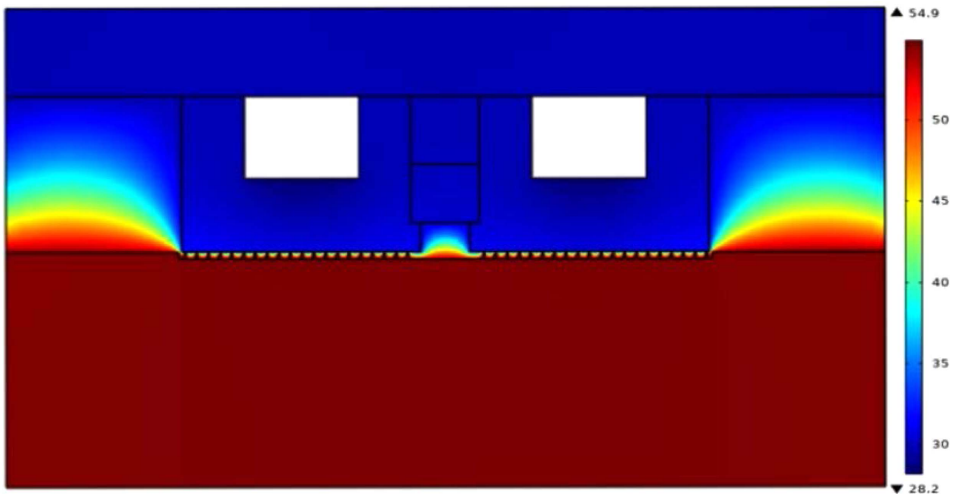


Fig. 11. (Color online) Two-dimensional temperature distribution contour map of the seal clearance under cooling condition.

shaft can only dissipate heat in a radially outward direction via its axial end - faces. Given that the thermal conductivity of air is considerably lower than that of metallic components like pole shoes and permanent magnets, the processes of heat transfer and dissipation are sluggish. This leads to temperatures surpassing 45 °C on both sides of the pole shoes and in the central air gap between them. Furthermore, the temperature gradually rises with an increase in the radial distance from the cooling water channel.

Under cooling condition, the heat transfer path of the sealing system is shown in Fig. 12. There exist three primary heat transfer paths within the sealed system. Path 1 involves the transfer from the magnetic fluid to the pole shoe and then to the cooling channel; Path 2 encompasses the transfer from the magnetic fluid to the shaft and then to the ambient air; and Path 3 includes the transfer from the magnetic fluid to the permanent magnet/air gap, followed by the housing, and finally to the ambient air. Path 1 depends on the pole shoe to conduct heat into the cooling channel, attaining an interface heat flux density of up to 8×10^3 W/m^2, which leads to outstanding heat transfer performance. In contrast, the heat flux densities related to Paths 2 and 3 are extremely low and can be disregarded during the analysis.

A parametric speed scan was carried out using MATLAB, with a scanning range from 500 to 8000 rpm and a sampling step of 500 rpm. The simulation results are shown in Fig. 13. This was done to acquire the steady-state temperature variation of the magnetic fluid under cooling conditions as a function of rotational speed. The temperature rise of the magnetic fluid does not demonstrate a linear relationship with rotational speed. As the speed increases, the rate of shear heating, which is influenced by the viscosity-temperature characteristics of the magnetic fluid, continuously decreases, leading to a

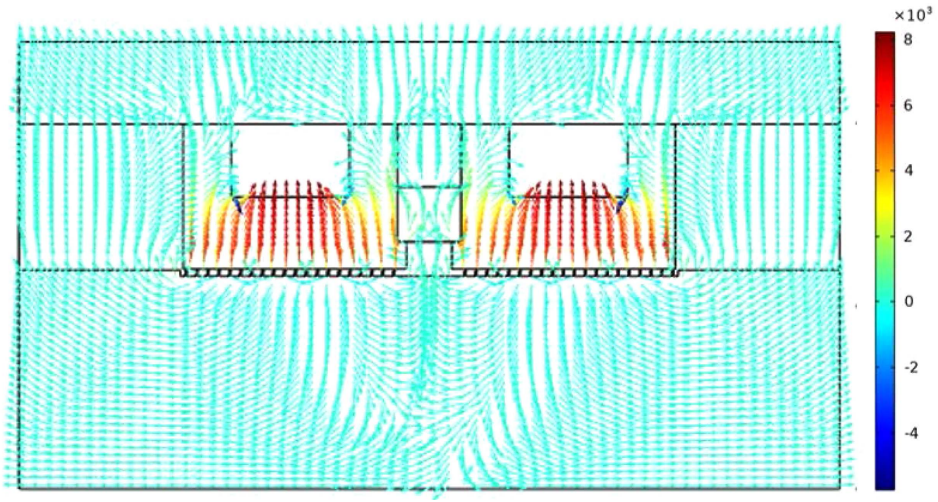


Fig. 12. (Color online) Vector map of heat flux density for the sealing device under cooling condition.

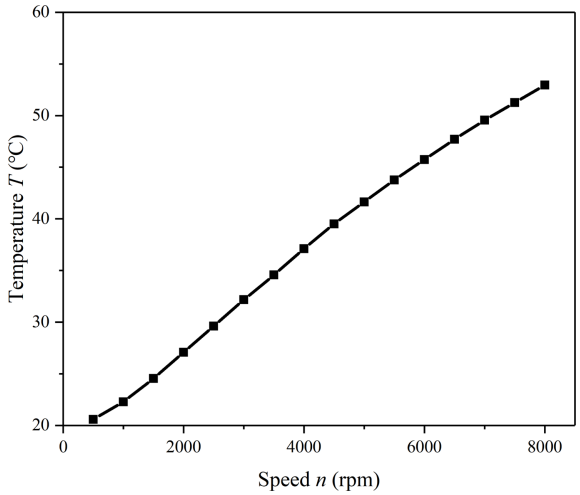


Fig. 13. Steady-state temperature of magnetic fluid as a function of rotational speed under cooling conditions.

progressive slowdown in the medium's temperature rise.

5.2. Experimental comparison

To validate the reliability of the temperature field numerical model, dynamic tests of magnetic fluid seals were carried out on a high-speed test platform to measure the thermal equilibrium temperatures of the magnetic fluid at different rotational speeds. The configuration of the experimental system and the operation procedure are detailed in the previous literature of the research group [19]. During the experiments, the temperature of the cooling water was kept constant at 24 °C. A comparison between the measured experimental data and the simulation results is presented in Fig. 14.

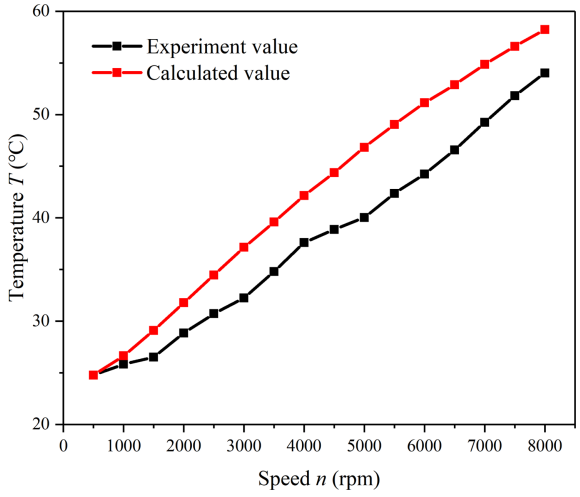


Fig. 14. (Color online) Experimental and calculated values of magnetic fluid temperature after stabilization at different rotational speeds.

As the shaft speed increases, the shear friction of the magnetic fluid within the sealing clearance intensifies, resulting in a substantial overall increase in the medium's steady-state temperature. A comparison between the simulation results and experimental measurements reveals minor discrepancies, with the simulated values generally being higher than the measured ones. This deviation mainly stems from two factors: firstly, the forced convection heat transfer coefficient for the cooling structure in the simulation model is an empirical estimate, which inherently introduces errors when compared to the actual heat transfer boundaries; secondly, when deriving the viscous dissipation heat generation formula, the axial effective contact length between the magnetic fluid and the pole teeth was simplified and equated to the geometric tooth width of the pole teeth, without considering the changes in the actual contact area caused by fluid flow under high-speed rotation. This idealized assumption diverges from the real operating conditions. These model simplifications and parameter estimation inaccuracies jointly lead to the simulated temperatures being slightly higher than the experimentally measured temperatures.

The simulation results indicate a 6% relative error when compared to experimental measurements. Nevertheless, the overall error remains within a reasonable range. The coupled viscous -thermal effect iterative simulation model developed in this study still exhibits good reliability. The acquired temperature field variation patterns can serve as a basis for design and offer reliable theoretical support for the thermal optimization of magnetic fluid sealing structures.

6. Conclusion

In this study, we carried out the programmatic modeling of the magnetic circuit for magnetic fluid seals by utilizing the COMSOL with MATLAB co - simulation platform. We derived the relational expression between the heat flux density of the viscous heat source and the temperature of the magnetic fluid. Subsequently, we developed an iterative simulation program for temperature field analysis and accomplished the cyclic correction of the heat source temperature and the solution of the steady-state magnetic fluid temperature. This paper performs a comparative analysis of the finite element temperature field for magnetic fluid seals under two conditions, namely cooling and no cooling. The conclusions offer a theoretical foundation for the thermal structural optimization design. At a rotational speed of 8000 rpm, the steady-state temperature in the seal clearance drops by 92 °C when cooled with 20 °C water as compared to the no cooling

condition. Although there is a 6% relative error between the simulation and experimental measurements, the overall error stays within an acceptable range, which indicates that this numerical model can reliably support the thermal structural optimization of magnetic fluid seals.

Declaration of conflicting interests

The authors declared no potential conflicts of interest with respect to the research, authorship, and/or publication of this article.

Funding

This work is funded by Science Research Project of Hebei Education Department (No. BJ2026292), Doctoral Research Startup Fund Project of Tangshan University (No. BC202423) and Hebei Provincial Natural Science Foundation General Project (No. E2024105049).

References

[1] J. Philip, Advances in colloid and interface science, Maharashtra **311**, 102810 (2023).
[2] Y. Mitamura, S. Takahashi, S. Amari, E. Okamoto, S. Murabayashi, and I. Nishimura, J. Artif. Organs **14**, 23 (2011).
[3] H. Urreta, G. Aguirre, and P. Kuzhir, International Journal of Precision Engineering and Manufacturing **19**, 495 (2018).
[4] B. K. Sreedhar, R. N. Kumar, and P. Sharma, Nuclear Engineering and Design **265**, 1166 (2013).
[5] R. E. Rosensweig, G. Miskolcz, and F. D. Ezekiel, Magnetic-fluid seals, Machine Design **40**, 145 (1968).
[6] P. A. Ryapolov, E. Shel'deshova, and E. B. Postnikov, J. Mol. Liq. **382**, 121887 (2023).
[7] R. E. Rosensweig, Ferrohydrodynamics, Cambridge University Press, Cambridge (1985) p. 43.
[8] B. M. Berkovsky, V. E. Fertman, V. K. Polevikov, and S. V. Isaev, Int. J. Heat Mass Transf. **19**, 981 (1976).
[9] V. E. Fertman, IEEE Trans. Magn. **16**, 352 (1980).
[10] M. O. Lutset and V. A. Starovoitov, IEEE Trans. Magn. **16**, 343 (1980).
[11] J. Kurfess and H. K. Muller, J. Magn. Magn. Mater. **85**, 246 (1990).
[12] Y. Chen, Z. Su, and J. Zhou, Nanomaterials **13**, 1019 (2023).
[13] S. A. Nesterov and V. D. Baklanov, Problems of the Regional Energetics **2**, 52 (2023).
[14] J. Yang, D. Li, and L. Jin, Magnetochemistry **11**, 18 (2025).
[15] J. Dong, D. Li, and Z. Li, J. Intell. Mater. Syst. Struct. **34**, 800 (2022).
[16] Z. Li, D. Li, J. Dong, H. Cui, and J. Yao, J. Magn. Magn. Mater. **545**, 168757 (2022).
[17] G. Kovács, S. K. Szürke, and S. Fischer, Batteries-Basel **11**, 1019 (2025).
[18] M. Szczech, IEEE Trans. Magn. **54**, 4600507 (2018).
[19] J. Dong, H. Lu, Z. Shen, and Z. Li, Magnetochemistry **12**, 12040042 (2026).